

Effective field theories for heavy quarkonium at finite temperature

Antonio Vairo*

Physik Department, Technische Universität München, 85748 Garching, Germany

E-mail: antonio.vairo@ph.tum.de

We discuss the recent development of effective field theories for quarkonium at finite temperature.

*8th Conference Quark Confinement and the Hadron Spectrum
September 1-6 2008
Mainz, Germany*

*Speaker.

1. Introduction

Experiments in past (SPS), present (RHIC) and future (LHC) colliders are attempting to recreate an early condition of the universe known as the quark-gluon plasma, where quarks and gluons exist without being bound into hadrons. Colliders explore the zero chemical potential region of the QCD phase diagram where lattice simulations indicate that a significant increase in the degrees of freedom happens above a certain critical temperature $T_c \approx 175$ MeV (for a recent review see [1]).

Heavy quarkonium dissociation has been proposed long time ago as a clear probe of the quark-gluon plasma formation in colliders through the measurement of the dilepton decay-rate signal [2]. Since higher excited quarkonium states are more weakly bound than lower ones, the expectation is that, as the temperature increases, quarkonium will dissociate subsequently from the higher to the lower states providing also a dynamical probe of the quark-gluon plasma formation (for some recent experimental data see [3]).

In order to study quarkonium properties in a thermal bath at a temperature T , the quantity to be determined is the quarkonium potential V , which dictates, through the Schrödinger equation

$$E \Phi = \left(\frac{p^2}{m} + V \right) \Phi, \quad (1.1)$$

the real-time evolution of the wave function Φ of a $Q\bar{Q}$ pair in the medium. In the full theory, V must come from a systematic expansion in $1/m$ (non-relativistic expansion), the leading term being the static potential, and in the energy E (ultrasoft expansion). The potential will encode all contributions from scales larger than E and smaller than m . If the temperature lies in this range, the potential will depend on it, if the temperature is smaller than or of the same order as E , the potential will be temperature independent.

The expansions in $1/m$ and E are best implemented in QCD by means of effective field theories (EFTs), very much in the same way as this has been done in order to describe quarkonium physics at zero temperature [4]. In the EFTs, the full dynamics will be more complicated than the Schrödinger equation (1.1), since the EFTs will account both for potential and/or non-potential interactions. However, Eq. (1.1) will provide the correct leading-order dynamics.

In the last two years, there has been a remarkable progress in constructing EFTs for quarkonium at finite temperature and in rigorously defining the quarkonium potential. In [5, 6], the static potential was calculated in the regime $T \gg 1/r \gtrsim m_D$, where m_D is the Debye mass and r the quark-antiquark distance, by performing an analytical continuation of the Euclidean Wilson loop to real time. The calculation was done in the weak-coupling resummed perturbation theory. The imaginary part of the gluon self energy gives an imaginary part to the static potential and hence a thermal width to the quark-antiquark bound state. In the same framework, the dilepton production rate for charmonium and bottomonium was calculated in [7, 8]. In [9], static particles in real-time formalism were considered and the potential for distances $1/r \sim m_D$ was derived for a hot QED plasma. The real part of the static potential was found to agree with the singlet free energy and the damping factor with the one found in [5]. In [10], a study of bound states in a hot QED plasma was performed in a non-relativistic EFT framework. In particular, the hydrogen atom was studied for temperatures ranging from $T \ll m\alpha^2$ to $T \sim m$, where the imaginary part of the potential becomes larger than the real part and the hydrogen ceases to exist. An EFT framework in real time and weak

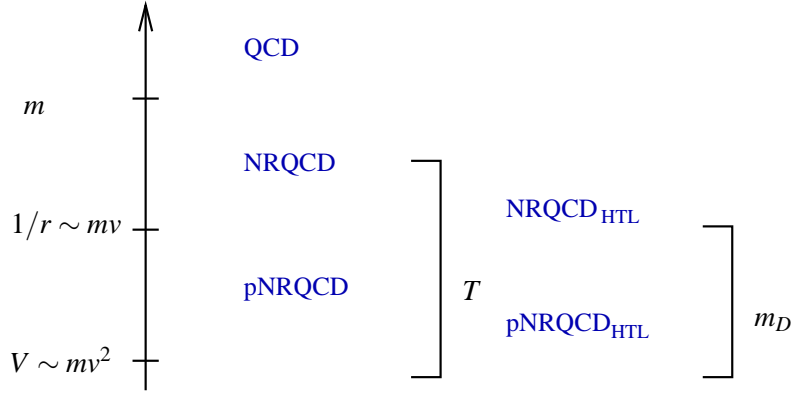


Figure 1: Quarkonium at finite temperature: energy scales and EFTs.

coupling for quarkonium at finite temperature was developed in [11]; in the rest of the presentation, we will follow closely that approach.

2. Scales and effective field theories

Quarkonium in a medium is characterized by different energy and momentum scales; there are the scales of the non-relativistic bound state (v is the relative heavy-quark velocity): m , the heavy quark mass, mv , the scale of the typical inverse distance between the heavy quark and antiquark, mv^2 , the scale of the typical binding energy or potential and lower energy scale, and there are the thermodynamical scales: the temperature T , the inverse of the screening length of the chromoelectric interactions, i.e. the Debye mass m_D and lower scales, which we will neglect in the following.

If these scales are hierarchically ordered, then we may expand physical observables in the ratio of the scales. If we separate explicitly the contributions from the different scales at the Lagrangian level this amounts to substituting QCD with a hierarchy of EFTs, which are equivalent to QCD order by order in the expansion parameters. At zero temperature the EFTs that follow from QCD by integrating out the scales m and mv are called respectively Non-relativistic QCD (NRQCD) and potential NRQCD (pNRQCD), see [4] for a review. We assume that the temperature is high enough that $T \gg gT \sim m_D$ holds but also that it is low enough for $T \ll m$ and $1/r \sim mv \gtrsim m_D$ to be satisfied, because for higher temperature the bound state ceases to exist. Under these conditions some possibilities are in order. If T is the next relevant scale after m , then integrating out T from NRQCD leads to an EFT that we may name $\text{NRQCD}_{\text{HTL}}$, because it contains the hard thermal loop (HTL) Lagrangian [12]. Subsequently integrating out the scale mv from $\text{NRQCD}_{\text{HTL}}$ leads to a thermal version of pNRQCD that we may call $\text{pNRQCD}_{\text{HTL}}$. If the next relevant scale after m is mv , then integrating out mv from NRQCD leads to pNRQCD. If the temperature is larger than mv^2 , then the temperature may be integrated out from pNRQCD leading to a new version of $\text{pNRQCD}_{\text{HTL}}$. The hierarchies of scales that lead to these different EFTs are schematically illustrated in Fig. 1. Note that, as long as the temperature is smaller than the scale being integrated out, the matching leading to the EFT may be performed putting the temperature to zero.

In the following we will also assume that $v \sim \alpha_s$, which is expected to be valid for tightly bound states: $\Upsilon(1S)$, J/ψ ,

The mass m is the largest scale in the system. This allows to integrate out m first and organize the EFTs as expansions in $1/m$. The leading order in the $1/m$ expansion corresponds to the static limit of NRQCD:

$$\mathcal{L} = -\frac{1}{4}F_{\mu\nu}^a F^{a\mu\nu} + \sum_{i=1}^{n_f} \bar{q}_i i\not{D} q_i + \psi^\dagger iD_0 \psi + \chi^\dagger iD_0 \chi, \quad (2.1)$$

where ψ (χ) is the field that annihilates (creates) the (anti)fermion; q_i are n_f light (massless) quark fields. Only longitudinal gluons couple to static quarks. The relevant scales in static NRQCD are: $1/r, V, \dots, T, m_D, \dots$.

Since we are interested in the real-time evolution of the heavy quark-antiquark pair, it is convenient to modify the contour of the partition function in order to allow for real times, see, for instance, [13]. In real time, the degrees of freedom double, modifying the propagators into 2×2 matrices. Despite this, the advantages are that the way in which calculations are carried out is very close to the one for $T = 0$ EFTs, moreover, in the static quark sector, the second degrees of freedom, labeled “2”, decouple from the physical degrees of freedom, labeled “1”. The technical reason for this is that the $[\mathbf{S}_Q^{(0)}(p)]_{12}$ component of a static quark propagator vanishes, hence the unphysical static quark fields “2” never enter in any physical amplitude, i.e. any amplitude that has the physical fields “1” as initial and final states. It is also very convenient to chose the Coulomb gauge: in Coulomb gauge, only transverse gluons carry a thermal part, but they do not couple to static quarks. Finally, also the static quark-antiquark potential has a 2×2 matrix structure, which reads

$$\begin{pmatrix} V & 0 \\ -2i\text{Im}V & -V^* \end{pmatrix}. \quad (2.2)$$

In the following, whenever we speak about the potential, we mean the physical one, i.e. the entry V in the above matrix.

3. Static quark antiquark at $T \lesssim V$

If the temperature is very low, $T \lesssim V$, then it does not affect the potential, which may be derived by integrating out the scale $1/r$ from (2.1). This leads to pNRQCD in the static limit, whose degrees of freedom are quark-antiquark states (color singlet S, color octet O), low energy gluons and light quarks. The Lagrangian is organized as an expansion in r :

$$\begin{aligned} \mathcal{L} = & -\frac{1}{4}F_{\mu\nu}^a F^{\mu\nu a} + \sum_{i=1}^{n_f} \bar{q}_i i\not{D} q_i + \text{Tr} \{ \mathbf{S}^\dagger (i\partial_0 - V_s) \mathbf{S} + \mathbf{O}^\dagger (iD_0 - V_o) \mathbf{O} \} \\ & + V_A \text{Tr} \{ \mathbf{O}^\dagger \mathbf{r} \cdot \mathbf{g} \mathbf{E} \mathbf{S} + \mathbf{S}^\dagger \mathbf{r} \cdot \mathbf{g} \mathbf{E} \mathbf{O} \} + \frac{V_B}{2} \text{Tr} \{ \mathbf{O}^\dagger \mathbf{r} \cdot \mathbf{g} \mathbf{E} \mathbf{O} + \mathbf{O}^\dagger \mathbf{O} \mathbf{r} \cdot \mathbf{g} \mathbf{E} \} + \dots \end{aligned} \quad (3.1)$$

At leading order in r , the singlet decouples from the octet and its equation of motion is $(i\partial_0 - V_s)\mathbf{S} = 0$. We may identify V_s and V_o with the singlet and octet potentials. They are Coulombic: $V_s(r) = -C_F \frac{\alpha_s}{r}$ and $V_o(r) = \frac{\alpha_s}{2N_c r}$ at leading order in α_s ($N_c = 3, C_F = 4/3$).

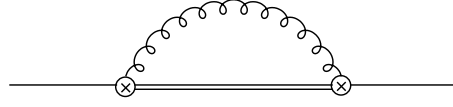


Figure 2: Single and double lines stand respectively for color singlet and color octet quark-antiquark propagators. The curly line stands for the chromoelectric correlator $\langle \mathbf{E}^a(t) \phi_{ab}(t, 0) \mathbf{E}^b(0) \rangle$, where ϕ_{ab} is a Wilson line in the adjoint representation, circles with cross stand for chromoelectric dipole interactions.

Thermal corrections do not affect the potential, but affect the static energy and the decay width through loop corrections. The leading correction is carried by the diagram shown in Fig. 2. The real part of the diagram gives the following thermal correction to the static energy

$$\delta E = \frac{2}{3} N_c C_F \frac{\alpha_s^2}{\pi} r T^2 f(N_c \alpha_s / (2rT)), \quad (3.2)$$

where $f(z) = \int_0^\infty dx \frac{x^3}{e^x - 1} \text{P} \frac{1}{x^2 - z^2} = \frac{z^2}{2} \left[\ln \frac{z}{2\pi} - \text{Re} \psi \left(i \frac{z}{2\pi} \right) \right] + \frac{\pi^2}{6}$. The imaginary part of the diagram gives the thermal width

$$\Gamma = \frac{N_c^3 C_F}{6} \frac{\alpha_s^4}{r} n_B(N_c \alpha_s / (2r)), \quad (3.3)$$

where $n_B(k^0) = 1/(e^{k^0/T} - 1)$ is the Bose statistical factor. Corrections coming from the scale m_D are suppressed by powers of m_D/T . The width Γ originates from the fact that thermal fluctuations of the medium at short distances may destroy a color-singlet $Q\bar{Q}$ into an octet plus gluons. This process is specific of QCD at finite T . We will call this process the singlet to octet break-up phenomenon; in QCD the corresponding diagrams are shown in Fig. 3.

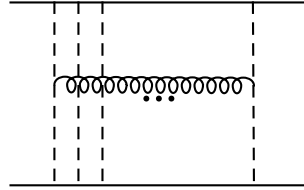


Figure 3: QCD diagrams responsible for the singlet to octet transition width in a thermal bath.

In the limiting case $T \ll V$, we have

$$\delta E = -\frac{8}{45} \pi^3 \frac{C_F}{N_c} r^3 T^4 = -\frac{4}{3} \pi \frac{C_F}{N_c} r^3 \langle \mathbf{E}^a(0) \cdot \mathbf{E}^a(0) \rangle_T, \quad (3.4)$$

and Γ is exponentially suppressed.

4. Static quark antiquark at $1/r \gg T \gg V$

In the situation $1/r \gg T \gg V$, integrating out T from pNRQCD modifies pNRQCD into a new EFT, pNRQCD_{HTL}. With respect to pNRQCD, the Yang–Mills sector of the pNRQCD_{HTL}

Lagrangian gets an additional hard thermal loop part [12], which modifies, for instance, the longitudinal gluon propagator at $k^0 = 0$ as

$$\frac{i}{\mathbf{k}^2} \rightarrow \frac{i}{\mathbf{k}^2 + m_D^2} + \pi \frac{T}{|\mathbf{k}|} \frac{m_D^2}{(\mathbf{k}^2 + m_D^2)^2}. \quad (4.1)$$

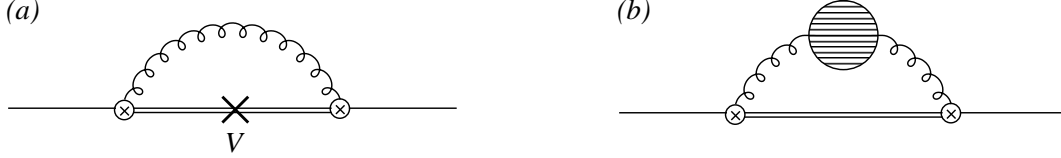


Figure 4: Diagrams contributing to the real part of the potential. The cross in diagram (a) means that we consider only one octet potential insertion into the free octet propagator; the shaded circle in diagram (b) stands for the gluon self-energy diagrams.

Also the potential in pNRQCD_{HTL} gets an additional thermal correction δV to the Coulomb potential of pNRQCD. The leading contribution to the real part of the color-singlet potential comes from the diagrams shown in Fig. 4 and reads

$$\text{Re } \delta V_s(r) = \frac{\pi}{9} N_c C_F \alpha_s^2 r T^2 - \frac{3}{2} \zeta(3) C_F \frac{\alpha_s}{\pi} r^2 T m_D^2 + \frac{2}{3} \zeta(3) N_c C_F \alpha_s^2 r^2 T^3. \quad (4.2)$$

The first term stems from diagram (a) and is of order $g^2 r^2 T^3 \times V/T$, the other ones stem from diagram (b) and are of order $g^2 r^2 T^3 \times (m_D/T)^2$.

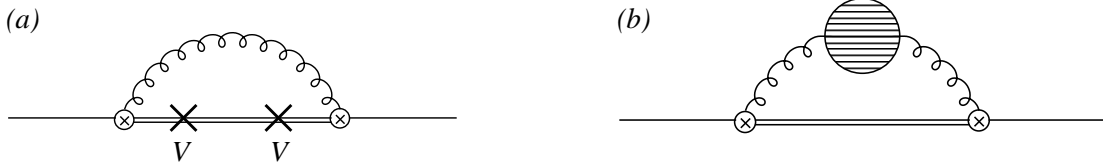


Figure 5: Diagrams contributing to the imaginary part of the potential. The two crosses in diagram (a) mean that we consider two octet potential insertions into the free octet propagator.

The leading contribution to the imaginary part of the color-singlet potential comes from the diagrams shown in Fig. 5 and reads

$$\begin{aligned} \text{Im } \delta V_s(r) = & -\frac{N_c^2 C_F}{6} \alpha_s^3 T + \frac{C_F}{6} \alpha_s r^2 T m_D^2 \left(\frac{1}{\epsilon} + \gamma_E + \ln \pi - \ln \frac{T^2}{\mu^2} + \frac{2}{3} - 4 \ln 2 - 2 \frac{\zeta'(2)}{\zeta(2)} \right) \\ & + \frac{4\pi}{9} \ln 2 N_c C_F \alpha_s^2 r^2 T^3. \end{aligned} \quad (4.3)$$

The first term stems from diagram (a) and is of order $g^2 r^2 T^3 \times (V/T)^2$, the other ones stem from diagram (b) and are of order $g^2 r^2 T^3 \times (m_D/T)^2$. The imaginary part of the diagram (a) may be traced back to the singlet to octet break-up phenomenon introduced above while the imaginary part of the diagram (b) is due to the imaginary part of the gluon self energy. This may be interpreted as due to the scattering of soft space-like gluons emitted by the heavy quarks with hard particles (gluons and light quarks) in the medium. In plasma physics, this phenomenon is known as Landau damping [5, 9].

Divergences appear in the imaginary part of the potential at order $g^2 r^2 T^3 \times (m_D/T)^2$, which have been regularized in dimensional regularization ($\varepsilon = (4-d)/2$, where d is the number of dimensions). They cancel in physical observables against loop corrections from lower energy scales. In order to illustrate the cancellation mechanism, let's consider the case $1/r \gg T \gg m_D \gg V$. Under this condition also the scale m_D contributes to the potential. Integrating out m_D from pNRQCD_{HTL} leads to an extra contribution δV_s to the potential coming from the diagram shown in Fig. 2 when the momentum flowing in the loop is of order m_D and consequently the gluon propagator is taken to be the HTL resummed gluon propagator as in Eq. (4.1). This extra contribution reads

$$\text{Re } \delta V_s(r) \sim g^2 r^2 T^3 \times \left(\frac{m_D}{T}\right)^3, \quad (4.4)$$

$$\text{Im } \delta V_s(r) = -\frac{C_F}{6} \alpha_s r^2 T m_D^2 \left(\frac{1}{\varepsilon} - \gamma_E + \ln \pi + \ln \frac{\mu^2}{m_D^2} + \frac{5}{3}\right). \quad (4.5)$$

The divergence in the imaginary part exactly cancels the one in (4.3).

Summing up the real and imaginary parts of the potential corrections obtained from the scales T and m_D , we end up with the thermal correction to the static energy δE and the thermal decay width Γ respectively:

$$\delta E = \frac{\pi}{9} N_c C_F \alpha_s^2 r T^2 - \frac{3}{2} \zeta(3) C_F \frac{\alpha_s}{\pi} r^2 T m_D^2 + \frac{2}{3} \zeta(3) N_c C_F \alpha_s^2 r^2 T^3, \quad (4.6)$$

$$\Gamma = -2 \text{Im } \delta V_s = \frac{N_c^2 C_F}{3} \alpha_s^3 T - \frac{C_F}{3} \alpha_s r^2 T m_D^2 \left(2\gamma_E - \ln \frac{T^2}{m_D^2} - 1 - 4 \ln 2 - 2 \frac{\zeta'(2)}{\zeta(2)}\right) - \frac{8\pi}{9} \ln 2 N_c C_F \alpha_s^2 r^2 T^3. \quad (4.7)$$

The (leading) non-thermal part of the static energy is the Coulomb potential $-C_F \alpha_s/r$. The thermal width has two origins. The first term comes from the thermal break up of a quark-antiquark color singlet state into a color octet state. The other terms come from imaginary contributions to the gluon self energy that may be traced back to the Landau-damping phenomenon. The first one is specific of QCD, the second one would also show up in QED. Having assumed $m_D \gg V$, the term due to the singlet to octet break up is parametrically suppressed by $(V/m_D)^2$ with respect to the imaginary gluon self-energy contributions. The $\ln T^2/m_D^2$ term is a remnant of the cancellation occurred between an infrared divergence at the scale T and an ultraviolet divergence at the scale m_D .

5. Static quark antiquark at $T \gg 1/r \gg m_D$

In the situation $T \gg 1/r \gg m_D$, integrating out T from static QCD leads to static NRQCD_{HTL}, which, at one loop, is static NRQCD with the Yang-Mills Lagrangian supplemented by the HTL Lagrangian. Subsequently, integrating out $1/r$ leads to a specific version of pNRQCD_{HTL} where the Coulomb potential gets corrections from HTL insertions. The leading real correction comes from the diagram shown in Fig. 6, which gives

$$\text{Re } \delta V_s(r) = -\frac{C_F}{2} \alpha_s r m_D^2. \quad (5.1)$$

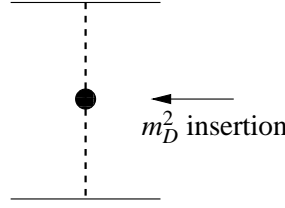


Figure 6: Leading real thermal correction to the potential. The black dot stands for the insertion of the real part of the HTL gluon self energy.

This is a correction proportional to $\alpha_s/r \times (rm_D)^2$.

The leading correction to the imaginary part of the potential comes from the diagrams shown in Fig. 7, which give

$$\text{Im } \delta V_s(r) = -\frac{N_c^2 C_F}{6} \alpha_s^3 T + \frac{C_F}{6} \alpha_s r^2 T m_D^2 \left(\frac{1}{\varepsilon} + \gamma_E + \ln \pi + \ln(r\mu)^2 - 1 \right). \quad (5.2)$$

The first term comes from diagram (a) in Fig. 7. It is proportional to $\alpha_s/r \times (rV)^2 \times (Tr)$ and its origin may be traced back to the singlet to octet break-up phenomenon. The other terms come from diagram (b) in Fig. 7. They are proportional to $\alpha_s/r \times (rm_D)^2 \times (Tr)$ and their origin may be traced back to the Landau-damping phenomenon.

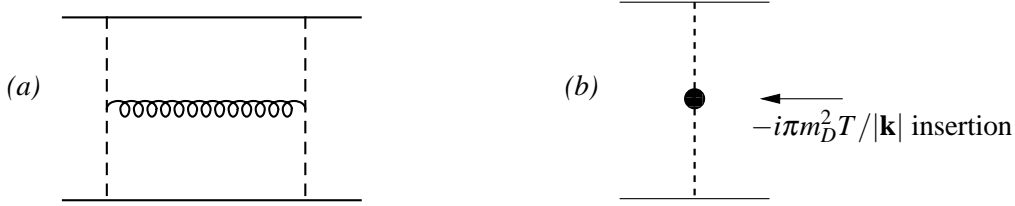


Figure 7: Leading contributions to the thermal decay width. Here, the black dot stands for the insertion of the imaginary part of the HTL gluon self energy.

Divergences appear in the imaginary part of the potential at order $\alpha_s/r \times (rm_D)^2 \times (Tr)$. They cancel in physical observables against loop corrections from lower energy scales. In order to illustrate the cancellation mechanism, let's consider the case $T \gg 1/r \gg m_D \gg V$, which is similar to the one discussed in the previous section. Integrating out m_D from pNRQCD_{HTL} leads to an extra contribution δV_s to the potential coming from the diagram shown in Fig. 2 when the momentum flowing in the loop is of order m_D and consequently the gluon propagator is taken to be the HTL resummed gluon propagator as in Eq. (4.1). These extra contributions are the same as in Eqs. (4.4) and (4.5).

Summing up the real and imaginary parts of the potential corrections obtained from the scales $1/r$ and m_D , we end up with the thermal correction to the static energy δE and the thermal decay width Γ respectively:

$$\delta E = -\frac{C_F}{2} \alpha_s r m_D^2, \quad (5.3)$$

$$\Gamma = \frac{N_c^2 C_F}{3} \alpha_s^3 T + \frac{C_F}{3} \alpha_s r^2 T m_D^2 \left(-2\gamma_E - \ln(rm_D)^2 + \frac{8}{3} \right). \quad (5.4)$$

The (leading) non-thermal part of the static energy is the Coulomb potential $-C_F \alpha_s/r$. Again the thermal width has two origins. The first term comes from the thermal break up of a quark-antiquark color singlet state into a color octet state. The other terms come from imaginary contributions to the gluon self energy that may be traced back to the Landau-damping phenomenon. Having assumed $m_D \gg V$, the term due to the singlet to octet break up is parametrically suppressed by $(V/m_D)^2$ with respect to the imaginary gluon self-energy contributions. The $\ln(rm_D)^2$ term is a remnant of the cancellation occurred between an infrared divergence at the scale $1/r$ and an ultraviolet divergence at the scale m_D .

It is in the situation $T \gg 1/r \gg m_D \gg V$ that quarkonium in the medium melts, if we assume that the melting condition is $E_{\text{binding}} \sim \Gamma$, where E_{binding} is the quarkonium binding energy. Using the above results, the condition gives $g^2/r \sim g^2 T m_D^2 r^2 \ln 1/(m_D r)$. For $1/r \sim m g^2$ and $m_D \sim g T$, this leads to the melting temperature $T_{\text{melting}} \sim m g^{4/3} (\ln 1/g)^{-1/3}$, where, assuming $g < 0.5$, we have neglected $\ln \ln 1/g$ with respect to $\ln 1/g$ [10, 14].

6. Static quark antiquark at $T \gg 1/r \sim m_D$

In the situation $T \gg 1/r \sim m_D$, integrating out T from static QCD leads to static NRQCD_{HTL}. Subsequently, both the scales $1/r$ and m_D have to be integrated out at the same time; this implies using HTL resummed gluon propagators in the matching procedure that leads to a new specific version of pNRQCD_{HTL}.



Figure 8: Diagram (a) shows the leading mass self energy contribution and diagram (b) the leading potential contribution to the static energy. Dashed lines stand for longitudinal HTL resummed gluon propagators.

The real part of the static energy is provided at leading order by the two diagrams shown in Fig. 8:

$$E = \text{Re} [2\delta m + \delta V_s(r)] = -C_F \alpha_s m_D - C_F \frac{\alpha_s}{r} e^{-m_D r}, \quad (6.1)$$

which is of order $\alpha_s m_D$. The result is in agreement with early results on δm and δV_s [15, 16].

The thermal decay width is provided at leading order by the three diagrams shown in Fig. 9:

$$\Gamma = \frac{N_c^2 C_F}{3} \alpha_s^3 T + 2C_F \alpha_s T \left[1 - \frac{2}{rm_D} \int_0^\infty dx \frac{\sin(m_D r x)}{(x^2 + 1)^2} \right]. \quad (6.2)$$

The first term is due to the singlet to octet break-up mechanism and is of order $\alpha_s m_D \times (Vr)^2 \times T/m_D$ the other ones, which were first derived in [5], are of order $\alpha_s m_D \times T/m_D \gg \alpha_s m_D$, i.e. larger than the real part of the energy (we recall that the binding energy is already of the same order as the decay width at the lower temperatures discussed in the previous section). The imaginary part of δm is minus twice the damping rate of an infinitely heavy fermion [17].

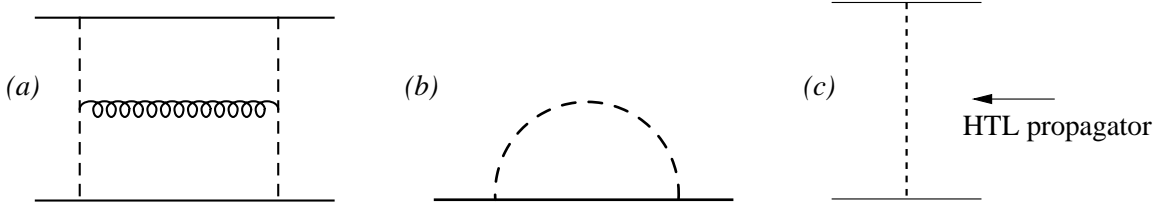


Figure 9: Diagram (a) is the leading diagram contributing to the singlet to octet break-up mechanism, diagram (b) contributes to the heavy quark damping rate and diagram (c) encodes the Landau-damping phenomenon. Dashed lines stand for longitudinal HTL resummed gluon propagators.

7. Conclusions

In a framework that makes close contact with modern effective field theories of non-relativistic bound states at zero temperature, we have discussed the real-time evolution of a static quark-antiquark pair in a medium of gluons and light quarks at finite temperature under the special assumption of weak coupling both for the non-relativistic and the thermal dynamics. For temperatures T ranging from values smaller to larger than the inverse distance of the quark and the antiquark we have derived the potential, the energy and the thermal decay width.

The derived potential, V_s , is neither the color-singlet quark-antiquark free energy nor the internal energy (whose practical definition, at variance with the $T = 0$ case, is plagued by many difficulties; for a recent critical discussion we refer to [18]). It has an imaginary part and may contain divergences that eventually cancel in physical observables.

The derived potential describes the real-time evolution of a quarkonium state in a thermal medium. At leading order, the evolution is governed by a Schrödinger equation. In an EFT framework, the potential follows naturally from integrating out all contributions coming from modes with energy and momentum larger than the binding energy. For $T < V$ the potential is simply the Coulomb potential. Thermal corrections affect the energy and induce a thermal width to the quarkonium state; these may be relevant to describe the in medium modifications of quarkonium at low temperatures. For $T > V$ the potential gets thermal contributions, which are both real and imaginary.

Two mechanisms contribute to the thermal decay width: the imaginary part of the gluon self energy induced by the Landau-damping phenomenon, and the quark-antiquark color singlet to color octet thermal break up. Parametrically, the first mechanism dominates for temperatures such that the Debye mass m_D is larger than the binding energy, while the latter dominates for temperatures such that m_D is smaller than the binding energy. Finally, it has been argued that quarkonium dissociation may be a consequence of the appearance of a thermal decay width rather than being due to the color screening of the real part of the potential; this follows from the observation that the thermal decay width becomes as large as the binding energy at a temperature at which color screening may not yet have set in.

Acknowledgments

I thank Nora Brambilla, Jacopo Ghiglieri and Péter Petreczky for collaboration on the work presented here.

References

- [1] H. Satz, *J. Phys. G* **32**, R25 (2006) [arXiv:hep-ph/0512217].
- [2] T. Matsui and H. Satz, *Phys. Lett. B* **178**, 416 (1986).
- [3] M. Leitch, “Quarkonium Measurements in PHENIX”, talk at Understanding QGP Through Spectral Functions and Euclidean Correlators, RBRC Workshop at BNL (2008).
- [4] N. Brambilla, A. Pineda, J. Soto and A. Vairo, *Rev. Mod. Phys.* **77**, 1423 (2005) [arXiv:hep-ph/0410047].
- [5] M. Laine, O. Philipsen, P. Romatschke and M. Tassler, *JHEP* **0703**, 054 (2007) [arXiv:hep-ph/0611300].
- [6] M. Laine, O. Philipsen and M. Tassler, *JHEP* **0709**, 066 (2007) [arXiv:0707.2458 [hep-lat]].
- [7] M. Laine, *JHEP* **0705**, 028 (2007) [arXiv:0704.1720 [hep-ph]].
- [8] Y. Burnier, M. Laine and M. Vepsalainen, *JHEP* **0801**, 043 (2008) [arXiv:0711.1743 [hep-ph]].
- [9] A. Beraudo, J. P. Blaizot and C. Ratti, *Nucl. Phys. A* **806**, 312 (2008) [arXiv:0712.4394 [nucl-th]].
- [10] M. A. Escobedo and J. Soto, arXiv:0804.0691 [hep-ph].
- [11] N. Brambilla, J. Ghiglieri, A. Vairo and P. Petreczky, *Phys. Rev. D* **78**, 014017 (2008) [arXiv:0804.0993 [hep-ph]].
- [12] E. Braaten and R. D. Pisarski, *Nucl. Phys. B* **337**, 569 (1990); *ibid.* **339**, 310 (1990); *Phys. Rev. D* **45**, 1827 (1992). J. Frenkel and J. C. Taylor, *Nucl. Phys. B* **334**, 199 (1990).
- [13] M. Le Bellac, “Thermal Field Theory”, *Cambridge, UK: Univ. Pr. (1996) 256 p.*
- [14] M. Laine, arXiv:0810.1112 [hep-ph].
- [15] E. Gava and R. Jengo, *Phys. Lett. B* **105**, 285 (1981).
- [16] S. Nadkarni, *Phys. Rev. D* **34**, 3904 (1986).
- [17] R. D. Pisarski, *Phys. Rev. D* **47**, 5589 (1993).
- [18] O. Philipsen, arXiv:0810.4685 [hep-ph].